Journal of Molecular Medicine
https://doi.org/10.1007/s00109-023-02401-9

ORIGINAL ARTICLE

Effects of different amosite preparations on macrophages, lung damages, and autoimmunity

Alain Lescoat[1,2] · Riccardo Leinardi[3] · Kévin Pouxvielh[1] · Yousof Yakoub[3] · Marie Lelong[1] · Amandine Pochet[3] · Erwan Dumontet[4] · Nessrine Bellamri[1] · Erwan Le Tallec[1,2] · Cristina Pavan[5,6] · Francesco Turci[5,6] · Christophe Paris[1,7] · François Huaux[3] · Valérie Lecureur[1,8]

Received: 27 June 2023 / Revised: 9 November 2023 / Accepted: 14 November 2023

Abstract

The underlying mechanisms of asbestos-related autoimmunity are poorly understood. As the size, surface reactivity, and free radical activity of asbestos particles are considered crucial regarding the health effects, this study aims to compare the effects of exposure to pristine amosite (pAmo) or milled amosite (mAmo) particles on lung damage, autoimmunity, and macrophage phenotype. Four months after lung exposure to 0.1 mg of amosite, BAL levels of lactate dehydrogenase, protein, free DNA, CCL2, TGF-β1, TIMP-1, and immunoglobulin A of pAmo-exposed C57Bl/6 mice were increased when compared to fluids from control- and mAmo-exposed mice. Effects in pAmo-exposed mice were associated with lung fibrosis and autoimmunity including anti-double-strand DNA autoantibody production. mAmo or pAmo at 20 μg/cm^2 induced a pro-inflammatory phenotype characterized by a significant increase in TNFα and IL-6 secretion on human monocyte-derived macrophages (MDMs). mAmo and pAmo exposure induced a decrease in the efferocytosis capacities of MDMs, whereas macrophage abilities to phagocyte fluorescent beads were unchanged when compared to control MDMs. mAmo induced IL-6 secretion and reduced the percentage of MDMs expressing MHCII and CD86 markers involved in antigen and T-lymphocyte stimulation. By contrast, pAmo but not mAmo activated the NLRP3 inflammasome, as evaluated through quantification of caspase-1 activity and IL-1β secretion. Our results demonstrated that long-term exposure to pAmo may induce significant lung damage and autoimmune effects, probably through an alteration of macrophage phenotype, supporting in vivo the higher toxicity of entire amosite (pAmo) with respect to grinded amosite. However, considering their impact on efferocytosis and co-stimulation markers, mAmo effects should not be neglected.

Key messages

- Lung fibrosis and autoimmunity induced by amosite particles depend on their physicochemical characteristics (size and surface)
- Inhalation exposure of mice to pristine amosite fibers is associated with lung fibrosis and autoimmunity
- Anti-dsDNA antibody is a marker of autoimmunity in mice exposed to pristine amosite fibers
- Activation of lung mucosa-associated lymphoid tissue, characterized by IgA production, after exposure to pristine amosite fibers
- Pristine and milled amosite particle exposure reduced the efferocytosis capacity of human-derived macrophages

Keywords Amosite fibers · Autoimmunity · Efferocytosis · Lung fibrosis · Macrophages

Introduction

As a result of the worldwide pandemic of asbestos-related diseases [1], the International Agency for Research on Cancer (IARC) of the World Health Organization (WHO) proved that all forms of asbestos were carcinogenic to humans [2]. Asbestos minerals were banned or strictly regulated by health protection organizations in many high-income countries, albeit asbestos—mainly chrysotile—is still used in middle- and low-income countries [3]. Although worldwide consumption of asbestos has globally decreased [4], the re-emergence of asbestos-related

Extended author information available on the last page of the article

Published online: 28 November 2023

diseases was observed and associated with unexpected sources or non-occupational situations [5] where potentially hazardous elongate mineral particles [6] are produced together with regulated asbestos minerals. The detrimental health effects of asbestos and asbestos-like mineral exposure include mesothelioma, lung cancer, and fibrosis, which can appear decades after exposure. Beyond such pulmonary disorders, the association between asbestos exposure and autoimmune diseases, characterized by autoantibody production, has also been reported [7–9]. Although dust-related autoimmunity is classically considered associated with chronic occupational exposure, acute occupational exposure and non-occupational exposure may also induce autoimmunity [10, 11]. Exposure to fibrous amphiboles, such as amosite and crocidolite, was shown to increase the production of autoantibodies [12]. However, the autoimmune effects of asbestos are still poorly understood in contrast to the large body of evidence collected on fibrosis or cancer.

The most robust paradigm in particle toxicology correlates three key physicochemical parameters of asbestos with their toxicity and health effects, i.e., the peculiar asbestiform morphology, the high biopersistence, and an ion-mediated surface reactivity [13, 14]. Currently, the WHO considers hazardous to humans only asbestos fibers characterized by the following morphometric characteristics: length (L) $\geq$ 5 µm, diameter (D) < 3 µm, and aspect ratio (L/D) > 3. However, indoor air samples usually contain more than 70% of short respirable asbestos fibers [15], i.e., the fibers characterized by L < 5 µm, D < 3 µm, and L/D > 3. Even if short asbestos fibers are mainly considered less harmful than long fibers, such a statement is still a matter of debate [16]. Therefore, short asbestos fiber pathogenicity still needs to be addressed, especially considering their high proportion in the air, which may lead to a non-negligible concentration and thereof exposure.

The major lung cells in contact with inhaled asbestos fibers are epithelial cells and alveolar macrophages. Macrophages can recognize fibers through scavenger receptors such as MARCO [17] and phagocyte them depending on their size and surface characteristics. Indeed, short fibers (< 5 µm in length) may be more easily cleared than long fibers (> 10 µm), which leads to an imperfect engulfment of fibers called "frustrated phagocytosis," favoring alveolar macrophage cell death, the release of reactive oxygen and nitrogen species, and subsequent recruitment of inflammatory cells. This chronic inflammation is also promoted by asbestos-induced activation of the NOD-like receptor family, pyrin domain-containing 3 (NLRP3) inflammasome, triggering the production of the inflammatory interleukin-1β (IL-1β) cytokine [18]. Asbestos-induced chronic inflammation in turn triggers the activation of fibroblasts and collagen deposition.

Despite some epidemiological studies suggesting an association between asbestos and autoimmunity, characterized by the production of anti-nuclear autoantibodies (ANA) [9, 19, 20], the underlying mechanisms are poorly understood. By contrast, the association between respirable crystalline silica and the development of systemic autoimmune diseases characterized by the production of ANA is well endorsed [21, 22]. Such effects may occur through cellular debris accumulation due to particle-induced apoptosis and a defect in their clearance in silica-exposed macrophages, leading to the release of intracellular components in the extracellular medium [23]. Efficient phagocytosis of apoptotic bodies by macrophages, a process called "efferocytosis", participates in immune silencing [24] by preventing the release of intracellular antigens, including self-DNA and DNA-associated proteins. Efferocytosis is impaired by silica exposure in vitro and in vivo, and such impairment of immune silencing could directly participate in silica-induced autoimmunity. The impact of asbestos exposure on efferocytosis and the links with autoimmunity in this context remain to be determined.

This study compared the effects of two amosite preparations including an unaltered sample of fibrous amosite and a sample of amosite that had been milled to produce shorter fibers and non-fibrous particles, both at the pulmonary and systemic levels, with a focus on immune responses, including autoimmunity and macrophage function, through in vivo and in vitro approaches.

Materials and methods

Mineral fibers

Milled amosite (mAmo) and pristine amosite (pAmo), kindly provided by F. Turci (Turin, Italy) originated in South Africa. The length range of pAmo was 2–100 µm, with more than 30% of fibers longer than 5 µm. The grinding of pAmo in a ceramic ball mill machine to mAmo led to (a) a significant reduction of fibrous particles (the majority of particles after grinding had an aspect ratio < 3) [25, 26] and (b) altered surface reactivity. Despite having a lower surface area than mAmo, pAmo bound more protein, had more free radical activity, and had more oxidized surface iron than mAmo [27]. A table comparing the major characteristics of mineral fibers is available in supp data 1. All samples were thermally treated at 200 °C for 3 h to remove any possible trace of endotoxin, and suspensions were prepared by sonication and manual vortexing in sterile phosphate-buffered saline (PBS) or water for in vivo and in vitro experiments, respectively.

Chemicals and reagents

Human recombinant cytokines IFNγ, IL-4, and IL-13 were purchased from PeproTech (Neuilly sur Seine, France), and human recombinant M – CSF was obtained from Miltenyi Biotec SAS (Paris, France). Lipopolysaccharide (LPS) from *E. coli* (serotype: 055:B5) and z-VAD-FMK were purchased from Sigma-Aldrich (St-Quentin Fallavier, France) and MedChemExpress (Clinisciences, Nanterre, France), respectively. Stock solutions of human recombinant cytokines were prepared in sterile distilled water containing 0.1% bovine serum albumin. z-VAD-FMK was dissolved in dimethyl sulfoxide (DMSO), and the control culture received the same dose of DMSO as their treated counterparts, without exceeding 0.2% (vol/vol).

Animals

Female C57BL/6 mice weighing 20 g, used at 8 weeks of age, were purchased from Janvier SAS (St Berthevin, France). Females were used because the incidence of systemic autoimmune diseases is higher in females than in males and because females are also exposed to mineral dust [11]. Animals were kept with sterile rodent feed and acidified water and housed in positive-pressure air-conditioned units (25 °C, 50% relative humidity) on a 12-h light/dark cycle. After acclimatization, the animals were exposed by oropharyngeal instillation to mAmo or pAmo fibers (100 µg) suspended in a volume of 50 µl of PBS-BSA. Vehicle controls were injected with an equal volume of PBS-BSA. Mice were then euthanized 4 months (120 days) after particle administration with an intraperitoneal injection of 12 mg sodium pentobarbital (Certa, Braine-l'Alleud, Belgium).

Bronchoalveolar lavage and lung sampling

The bronchoalveolar lavage (BAL) was performed by cannulating the trachea and infusing the lungs with 1 ml of 0.9% NaCl four times. The BAL fluid was centrifuged at 280 g at 4 °C for 10 min using a 5804R centrifuge (Eppendorf, Hamburg, Germany), and the cell-free supernatant was used for biochemical measurements. After resuspension of the pellet in PBS, total BAL fluid cells were counted (at least 200 cells) in Turch (crystal violet 1%, acetic acid 3%) and then pelleted onto glass slides by cyto-centrifugation for differentiation by light optical microscopy after Diff-Quick staining (Baxter, Lessines, Belgium). Total proteins and lactate dehydrogenase (LDH) activity were assessed on BAL fluid as previously described [28]. BAL fluid content of double-stranded DNA (dsDNA) was measured using the Quant-iT PicoGreen dsDNA reagent (Invitrogen, Thermo Fisher Scientific, Courtaboeuf, France), according to the manufacturer's protocol.

Quantification of total lung collagen and BAL cytokines

Collagen deposition was estimated by measuring hydroxyproline (OH-proline) content in lung homogenates and tissue inhibitor of metalloproteinase (TIMP-1) content in BAL fluids. Hydroxyproline was assessed by high-pressure liquid chromatography analysis on hydrolyzed lung homogenates (6 N HCl at 108 °C during 24 h) as previously described [29]. Active TGF-β1, TIMP-1, and CCL2 levels were assessed by ELISA on BAL fluids according to manufacturers' instructions (R&D Systems, Minneapolis, USA). Total Ig-G, Ig-A, and Ig-M were measured using an Invitrogen Uncoated ELISA kit (Thermo Fisher Scientific).

Lung histology

Lungs were instilled and perfused with 0.9% NaCl, and the superior-left lung lobe was fixed in a 3.6% formaldehyde solution (Sigma-Aldrich) for one night. Sections embedded in paraffin were stained with hematoxylin and eosin (H&E, nucleus, and cytoplasm staining). Images were acquired with a slide scanner SCN400 (Leica, Diegem, Belgium) and processed with Tissue Image Analysis 2.0 (Leica).

Preparation of human monocyte-derived macrophages (MDMs)

Monocytes, selected after a 1-h adhesion step, were differentiated into MDM for 6 days using M – CSF (50 ng/ml) in RPMI 1640 medium GlutaMAX (Gibco, Life Technologies SAS, Courtaboeuf, France) supplemented with antibiotics (20 IU/ml penicillin and 20 µg/ml streptomycin (Thermo Fisher Scientific) and 10% heat-inactivated fetal bovine serum (FBS, Lonza, Levallois-Perret, France), as previously described [30]. After 6 days, the supernatant of cells was removed and replaced with a medium containing 5% of heat-inactivated FBS and M – CSF (10 ng/ml). These cells corresponding to M0-MDMs were then exposed to mAmo or pAmo from 0 to 50 µg/cm^2. For the inflammasome experiment, M0-MDMs were pre-incubated with 10 ng/ml of LPS in the presence or absence of 10 µm of z-VAD-FMK before amosite fibers. According to experiments, conditioned media were removed and stocked at – 20 °C for ELISA analysis, whereas the cells were washed and harvested for RNA extraction or flow cytometry analysis.

Evaluation of cell viability, cytokine/chemokine levels, and caspase-1 activity

Cell viability was assessed with a CyQUANT assay (Invitrogen, Thermo Fisher Scientific). MDMs plated at 2×10^5 cells/cm^2 were exposed to different concentrations of fibers

from 0 to 50 µg/cm^2 for 4 h or 24 h. After particle exposure, CyQUANT was added to MDMs in a complete medium and incubated for 1 h at 37 °C, and the supernatant was read with a spectrofluorimeter SPECTROStar OMEGA (BMG Labtech, Champigny s/Marne, France) using appropriate wavelengths (485/540 nm).

Levels of human IL-1β, IL-6, IL-8, and TNFα secreted in MDM culture media were quantified by ELISA using specific Duoset ELISA development system kits (R&D Systems).

Caspase-1 activity was quantified by luminescence using the Caspase-Glo 1 inflammasome assay according to the recommendations of providers (Promega, Charbonnières-les-Bains, France) on an Enspire 2300 luminometer (Perkin-Elmer, Waltham, MA, USA).

Cell surface receptor and marker analyses by flow cytometry

Phenotypic analysis of MDMs was performed using flow cytometric direct immunofluorescence. After washing and detachment using Accutase™ (BioLegends, Paris, France), cells were stained with Fixable Viability Stain 780 (BD Biosciences, Le Pont de Claix, France) for 10 min at room temperature to measure viability and exclude dead cells from the analysis. MDMs were first blocked in PBS supplemented with 2% FBS solution and with FcR blocking reagent (Miltenyi Biotec SAS) for 10 min at room temperature to avoid nonspecific binding, and then re-suspended and incubated with specific antibodies or appropriate isotype controls for 30 min at 4 °C. Cells were washed with PBS, collected by centrifugation (2500 rpm for 5 min), and then analyzed on a LSR II cytometer (BD Biosciences) and FlowLogicTM software (Miltenyi Biotec SAS). The phenotypic characterization of viable MDMs was performed using the following antibodies: BUV395 anti-MHCII, BV421 anti-CD200R, BV605 anti-CD80, BB515 anti-CD206, PE anti-CD163, and APC anti-CD86, their respective isotype controls, as recommended by BD Biosciences (Le Pont de Claix, France). Results are expressed as the mean ratio of median fluorescence intensity (MFI) calculated as follows: MFI (mAb of interest)/MFI (isotype control mAb).

Phagocytosis assays by flow cytometry

MDMs plated in 12-well tissue culture plates were exposed to fluorescent YG beads (Fluoresbrite™ Plain YG 1.0 Micron Microsphere, Polysciences, Warrington, USA) in a 10:1 ratio (fluorescent beads/MDM) for 45 min at 37 °C or 4 °C in a 5% CO_2 humidified incubator. Some M0-MDMs were pre-treated with 5 µm cytochalasin D (Sigma-Aldrich) for 1 h, thus acting as a negative control as cytochalasin D inhibits actin polymerization required for engulfment. After phagocytosis, MDMs were washed, detached, and stained for viability as already detailed above before YG fluorescence quantification on the cytometer. Results are expressed as the percentage of phagocytosis calculated as follows: % fluorescent MDMs (37 °C) – % fluorescent MDMs (4 °C).

Efferocytosis assays by real-time fluorescence microscopy

Human Jurkat CD4 T-lymphocyte cells (1.10^6 cells/ml), cultured in RPMI 1640 Glutamax culture medium with 10% FBS, 20 IU/ml penicillin, and 20 µg/ml streptomycin, were exposed for 4 h to 10 µM camptothecin (Sigma-Aldrich) to induce apoptosis as previously described [31]. Apoptotic Jurkat cells were then stained for 15 min with 250 ng/ml pHrodo (IncuCyte® pHrodo® Red Cell Labeling Kit, Sartorius, Ann Arbor, USA), washed, and added to MDMs plated in 96-well-tissue culture plates in a 10:1 ratio (apoptotic cells/MDM) for 180 min at 37 °C in a 5% CO_2 humidified incubator. The engulfment efficiency of MDMs was quantified by real-time fluorescence microscopy (IncuCyte® Live-Cell Analysis System, Sartorius), measuring the total integrated red intensity (ex:560 nm/em:585 nm) of labeled Jurkat cells when entering the acidic phagosome every 15 min. The mean fluorescence intensity of phagocytosed Jurkat cells after 90 min is used to compare the efferocytosis level.

Statistical analysis

Data are presented as means ± standard error on the mean (SEM). Comparison among more than 2 groups was performed by repeated measure analysis of variance for paired or one-way analysis of variance, followed by Dunnett's or the Newman–Keuls multiple comparison post-hoc test. Depending on conditions and Gaussian distribution, Student's *t*-test, paired *t*-test, or the Mann–Whitney test were used to compare the 2 groups. A $p < 0.05$ was considered significant. Data analyses were performed with GraphPad Prism 5.0 software (GraphPad Software, La Jolla, CA, USA).

Results

Lung and systemic effects of mAmo and pAmo in mice

Oropharyngeal instillation of pAmo resulted in leukocyte accumulation in the airways, which was characterized by a significant increase in neutrophils and macrophages 120 days after fiber exposure. By contrast, no increase in the count number of any leucocyte was found in BAL fluid after mAmo exposure (Table 1). As compared to vehicle- or

Table 1 Cell counts in the BAL fluids mice after 120 days of oropharyngeal instillation of milled Amosite (mAmo), pristine Amosite (pAmo) or PBS (Control)

	mean ± SEM	differential cell counts (number 10^3/ml)			
group	**Total cell number (10^6/ml)**	**Macrophages**	**Neutrophils**	**Lymphocytes**	**Eosinophils**
after 120 days					
PBS	31.0 + 2.7	28.8 + 2.4	1.7 + 0.6	0	nd
mAmo	31.2 + 4.2	28.0 + 3.5	2.7 + 0.5	0.5 + 0.2	nd
pAmo	73.0 + 18.1 *$	59.2 + 14.9 *$	10.2 + 3.1**$	1.1 + 0.6	nd

nd: not detected

* significantly different ($p < 0.05$) from PBS control

** significantly different ($p < 0,01$) from PBS control

$ significantly different ($p < 0.05$) from mAmo

mAmo-exposed mice, pAmo exposure resulted in a significant increase in LDH (Fig. 1a) and protein release, suggesting a loss of lung permeability with an increase in inflammatory mediators (Fig. 1b) and of the chemokine CCL2/MCP-1 that chemoattracts CCR2-positive monocytes (Fig. 1c).

By contrast to mAmo, pAmo exposure significantly increased active TGF-β (Fig. 1d) and tissue inhibitor of matrix metalloproteinase-1 (TIMP-1) releases as compared to control and mAmo (Fig. 1e), two makers of fibrosis. Exposure to pAmo (not mAmo) tended to increase hydroxyproline content when compared to control (Fig. 1f), indicating increased collagen formation by activated fibroblasts. As shown in Fig. 1g, pAmo exposure induced the development of fibrotic areas characterized by reduced alveolar spaces with thickening of alveolar walls, in contrast to control and mAmo-exposed mice.

As LDH release is associated with cell death, we hypothesized that pAmo-induced epithelial cell death [32], through the release of cell content in the extracellular microenvironment, exhibited antigenicity and induced a humoral immune response. Therefore, we examined immunoglobulin (Ig) levels in the BAL fluids (BALF) of mice. Total IgG and IgM levels did not differ among groups (Fig. 2a). By contrast, mean levels of IgA were significantly increased in BALF of pAmo-exposed mice as compared to vehicle- or mAmo-exposed mice, suggesting activation of lung mucosal immunity (Fig. 2a). A significant increase in free DNA levels in BALF (Fig. 2b) and of anti-double-stranded (ds)-DNA autoantibody concentration was also observed in the serum of pAmo-exposed mice in comparison to control and mAmo-exposed mice (Fig. 2c).

Overall, these results demonstrated that, in contrast to mAmo, inhaled pAmo-induced chronic airway inflammation (CCL2), lung fibrosis (TGF-β, TIMP-1, and hydroxyproline quantifications and lung histology), lung mucosal immunity (IgA secretion), and systemic autoimmunity (presence of serum dsDNA autoantibodies) in mice.

Comparative effects of mAmo and pAmo fibers on human MDM phenotype and functions

As alveolar macrophages, and especially monocyte-derived macrophages, are thought to play a key role in the development of asbestos-induced lung fibrosis [33], the model of human monocyte-derived macrophages (MDM) is well adapted to study and compare the cellular effects of the two different preparations of amosite. As particle exposure may alter the phenotype (M0, M1, and M2) of human MDM [34], we analyzed the phenotype and the phagocytic functions of MDM exposed to mAmo and pAmo.

The evaluation of fiber toxicity towards human MDM reveals a significant decrease in cell viability in cells exposed to 33 µg/cm^2 or to 25 µg/cm^2 4 h or 24 h post-exposure to mAmo, respectively (Fig. 3a), whereas pAmo exposure was cytotoxic only 24 h post-exposure with a concentration of 50 µg/cm^2 (Fig. 3b). The absence of cell toxicity from exposure to mAmo and pAmo at 20 µg/cm^2 for 24 h was confirmed by flow cytometry (Fig. 3c). Based on these data, we selected 20 µg/cm^2 of mAmo and pAmo for the next in vitro experiments.

Phenotype and activated states (inflammatory or M1 type and fibrotic or M2 type) of macrophages are validated by the up- or down-expression of specific markers. A significant down-expression of the endocytic receptor for hemoglobin-haptoglobin complex (or CD163) well known as a fibrotic M2 marker was found in MDM exposed to mAmo and pAmo, similar to M1-polarized MDM (Fig. 4a). The expression of the MHCII marker was also significantly reduced in the presence of mAmo but not with pAmo when compared to M0-MDM. No significant alteration of the specific M1 marker CD80 or the specific M2 marker CD200R was found after exposure to mAmo or pAmo (Fig. 4a). As the expression of CD86 (M1 markers) tended to decrease in mAmo-exposed MDM (Fig. 4a), we explored the percentage of cells expressing selected M1 markers. A significant decrease in

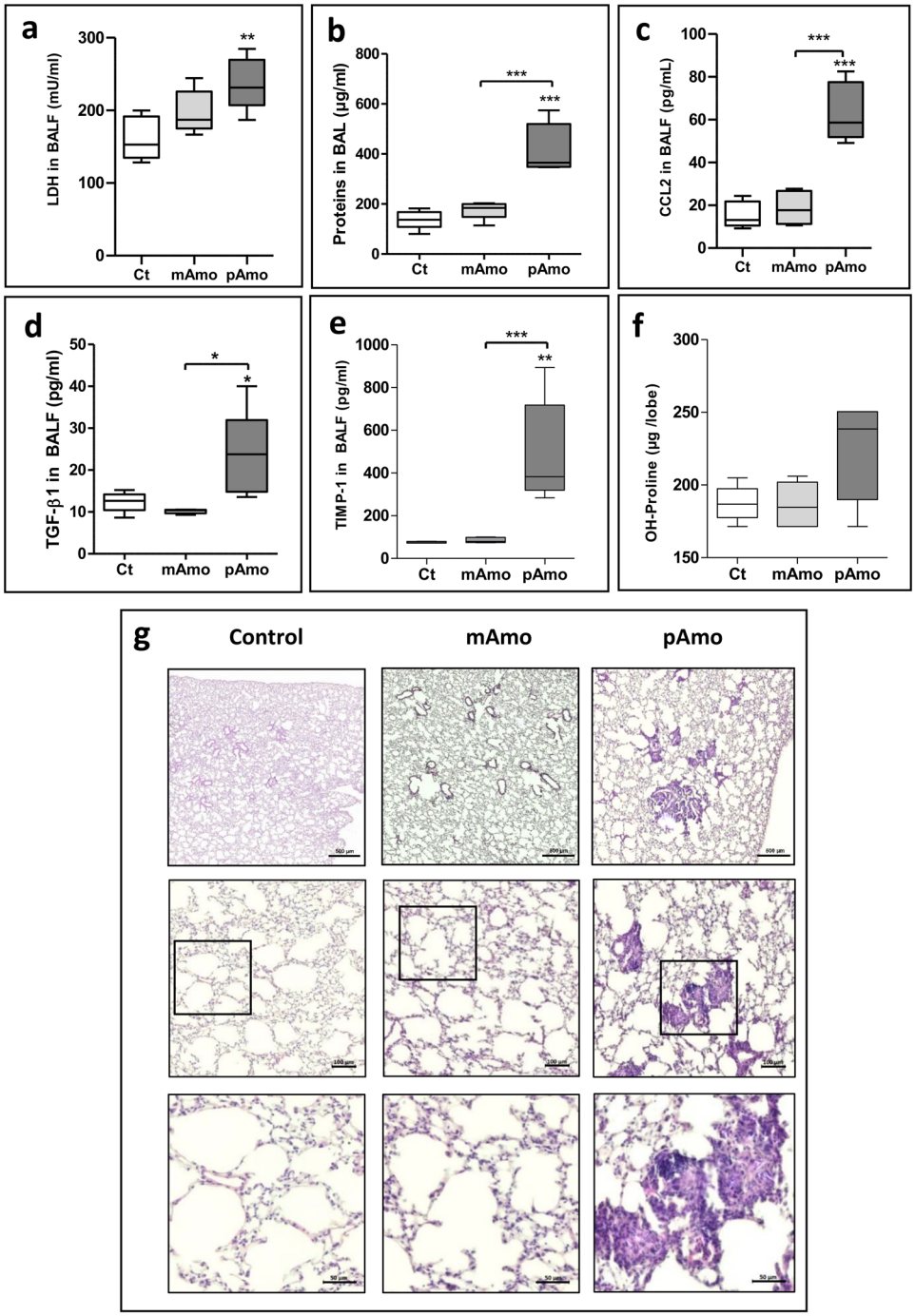

Fig. 1 Comparison of mAmo and pAmo exposures on lung inflammation and fibrosis. BAL fluids and lung were harvested at day 120 from control-, mAmo-, or pAmo-treated mice and analyzed for LDH release expressed in mU/ml (**a**), protein levels expressed in µg/ml (**b**), CCL2 (**c**), active TGF-β1 (**d**), and TIMP-1 (**e**) secretions expressed in pg/ml and for hydroxyproline content expressed in µg/lobe (**f**). Data represented the mean ± SEM with $n = 5$. $^{**}p < 0.01$, $^{***}p < 0.001$. Microscopic views at different magnifications of representative lung sections from control-, mAmo-, or pAmo-treated mice at day 120 using bright light. The bar scale represents 500 µm (**g**)

the percentage of cells positive for both CD86 and MHCII was found in comparison to M0-MDM or pAmo-exposed MDM (Fig. 4b), suggesting lower antigen presentation abilities of mAmo-exposed MDM.

The quantification of some key pro-inflammatory cytokines showed that the secretion levels of TNFα and IL-8 were significantly induced in supernatants of MDM exposed to mAmo and pAmo at 20 µg/cm^2 in comparison to M0-MDM, whereas IL-6 secretion was significantly increased only in mAmo-exposed MDM when compared to untreated and to pAmo-exposed MDM (Fig. 5a). The secretion levels of the M2a chemokine CCL18 were not modified by fiber exposure in vitro (data not shown). As asbestos is well known to assemble the NLRP3 inflammasome complex and to activate caspase-1, resulting in the conversion of pro-IL-1β to its mature form [18], we compared the effects of particles on caspase-1 activity and IL-1β release by MDMs primed by LPS. Caspase-1 activity (Fig. 5b) and IL-1β

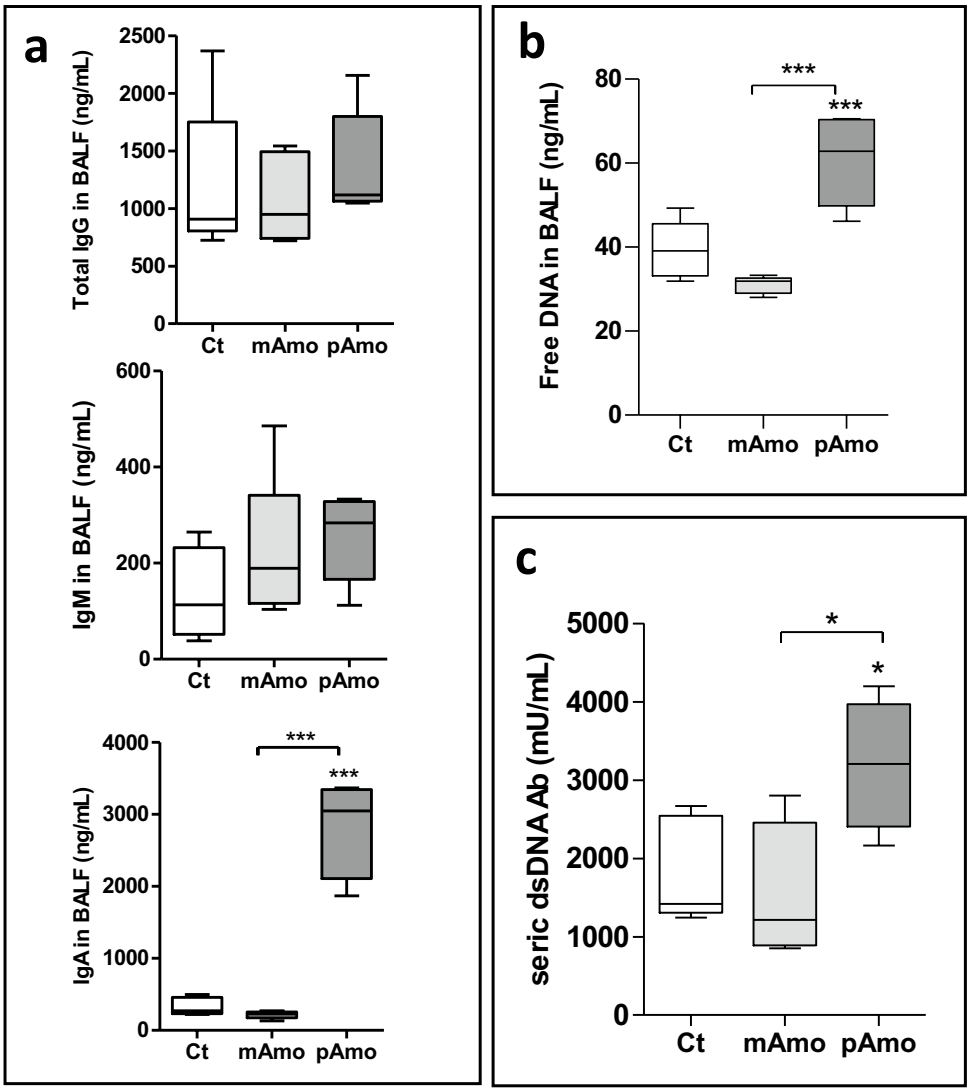

Fig. 2 Comparison of immune response to mAmo and pAmo exposure. BAL fluids and lung tissue were harvested at day 120 from control-, mAmo-, or pAmo-treated mice and analyzed for immunoglobulin IgG, IgA, and IgM (**a**) and for free DNA content expressed in ng/ml (**b**). Double-strand DNA antibody concentrations, expressed in mU/ml, were analyzed in the sera of mice (**c**). Data represented the mean ± SEM with $n = 5$. $^{*}p < 0.05$, $^{***}p < 0.001$

secretion were induced in pAmo-exposed cells (Fig. 5c). IL-1β secretion in the supernatants of mAmo-exposed MDM was increased, but not enough to reach a significant level. The role of the NALP3 inflammasome in IL-1β secretion after pAmo exposure was confirmed by the capacity of z-VAD-FMK, a caspase-1 inhibitor, to significantly reduce IL-1β levels (Fig. 5c).

As ineffective efferocytosis could contribute to autoimmunity [24] and as mineral particles such as crystalline silica decrease the efferocytosis capacities of macrophages [30], we assessed the effects of asbestos exposure on the efferocytosis capacities of macrophages. Human MDM capacities to phagocyte apoptotic cells (efferocytosis) were decreased when cells were exposed to mAmo or pAmo particles, without significant difference between fiber types (Fig. 6a), whereas exposure to non-toxic tungsten particles used as a negative control had no effect on efferocytosis [23]. By contrast, the phagocytosis of fluorescent beads by MDMs exposed to mAmo or pAmo was not reduced, contrary to those exposed to the potent actin polymerization inhibitor cytochalasin D (Fig. 6b).

Altogether, in vitro exposure of human MDM to amosite fibers induced a pro-inflammatory phenotype which differed between amosite preparations in IL-6 and IL-1β secretions, but that was associated for both of them with a decrease in the efferocytosis capacities of human MDM.

Discussion

Pathologic responses to toxicants depend on the dose, the duration of exposure, and their physical and chemical properties, notably their size, which are closely linked to their potential surface reactivity. Our study reveals for the first time that milling of amosite altering size, surface characteristics, and free radical release of amosite fibers [26, 27] have an impact on the development of autoimmunity as only long-term pAmo-exposed mice had increased levels of serum

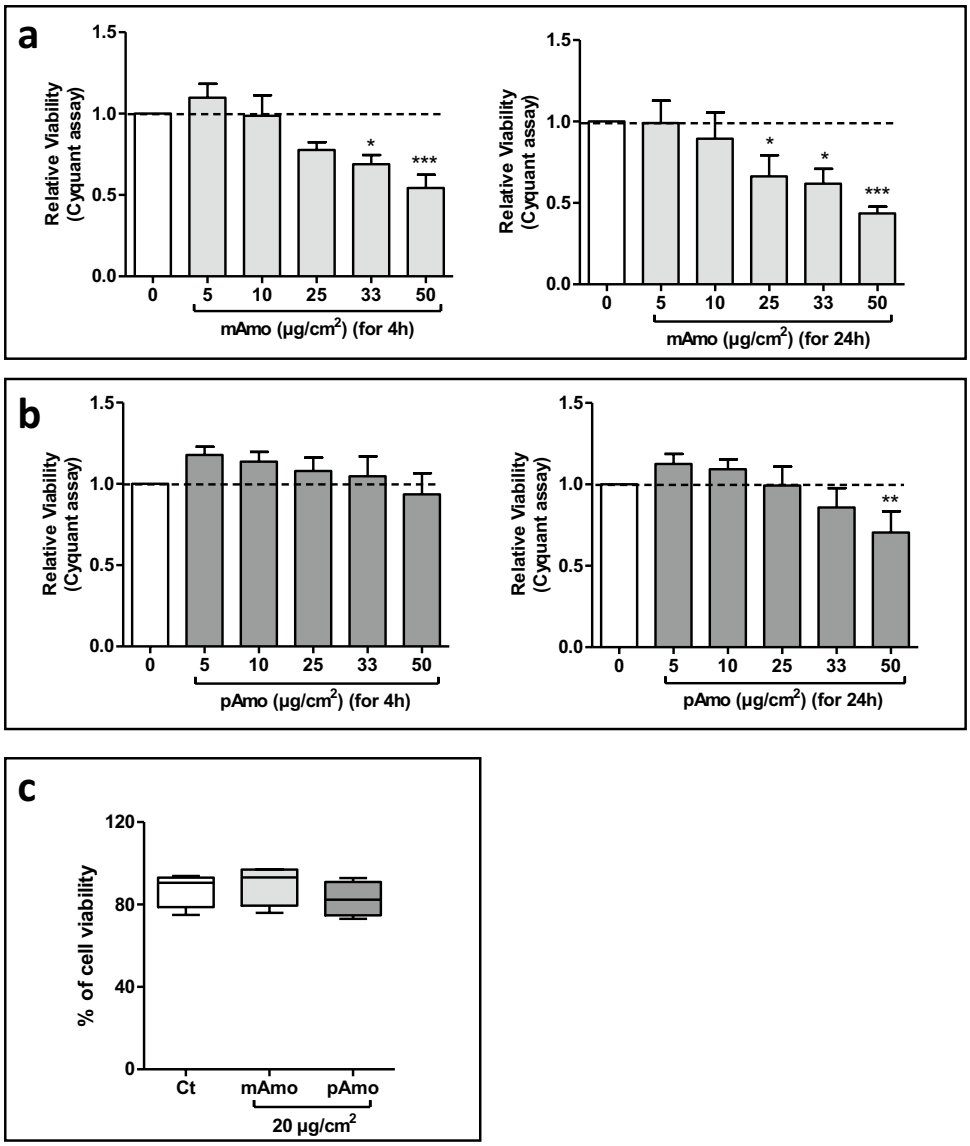

Fig. 3 Evaluation of the cell toxicity of mAmo and pAmo exposure in monocyte-derived macrophages (MDMs). MDMs were exposed to mAMo (**a**) or pAmo (**b**) from 5 to 50 µg/cm^2. After 4 h and 24 h of exposure time, cell viability was evaluated using the CyQUANT assay as described in the "Materials and methods" section. Data were expressed relative to untreated cells, arbitrarily set at a value of 1 unit, and are the mean ± SEM of 6 independent experiments. MDMs were exposed to mAmo or pAmo at 20 µg/cm.^{2} for 24 h (**c**), and cell viability was then evaluated by excluding the Fixable Viability Stain 780-positive cells by flow cytometry analysis as described in the "Materials and methods" section. Data were expressed relative to untreated cells and are the mean ± SEM of 4 independent experiments. *$p < 0.05$, **$p < 0.01$, ***$p < 0.001$

anti-dsDNA autoantibodies. Furthermore, our data support a higher impact of pAmo on lung health compared to mAmo, as pAmo exposure was characterized by increased inflammation and increased fibrosis in mice exposed to pAmo as compared to mAmo. Such differences could be linked to the differential impact of asbestos on macrophage phenotypes and functions.

Asbestos exposure is well known to induce inflammatory responses. In this study, we showed that long-term exposure to pAmo, by contrast to mAmo, increased the recruitment of inflammatory cells such as neutrophils and macrophages in accordance with higher secretion levels of the macrophage chemoattractive CCL2/MCP-1 chemokine in BALF. This continuing immune cell presence in BALF suggests ongoing injury of pAmo as compared to mAmo that could be related to the insolubility of amphibole in body fluids [35] and therefore to their persistency in lung tissues due to, at least in part, a "frustrated phagocytosis" by macrophages [36]. Moreover, phagocytosis of long fibers seems more aggressive, favoring lysosomal membrane rupture and a subsequent release of cathepsin D that results in NLRP3 activation [37]. These results are supported by our data showing a higher increase in activated caspase-1 and the process of maturation of pro-IL-1β to the mature and biologically active form of IL-1β by pAmo as compared to mAmo. In agreement with this result, previous studies showed higher activation of the NLRP3 inflammasome in LPS-primed macrophages by long carbon nanomaterials as compared to short [38].

In addition to the secretion of pro-inflammatory markers, human macrophages exposed to mAmo and pAmo showed, similarly to pro-inflammatory M1 macrophages and to macrophages exposed to crystalline silica [23], a lower expression of membrane CD163 and a scavenger receptor involved in the phagocytic ability of cells. The down-expression of

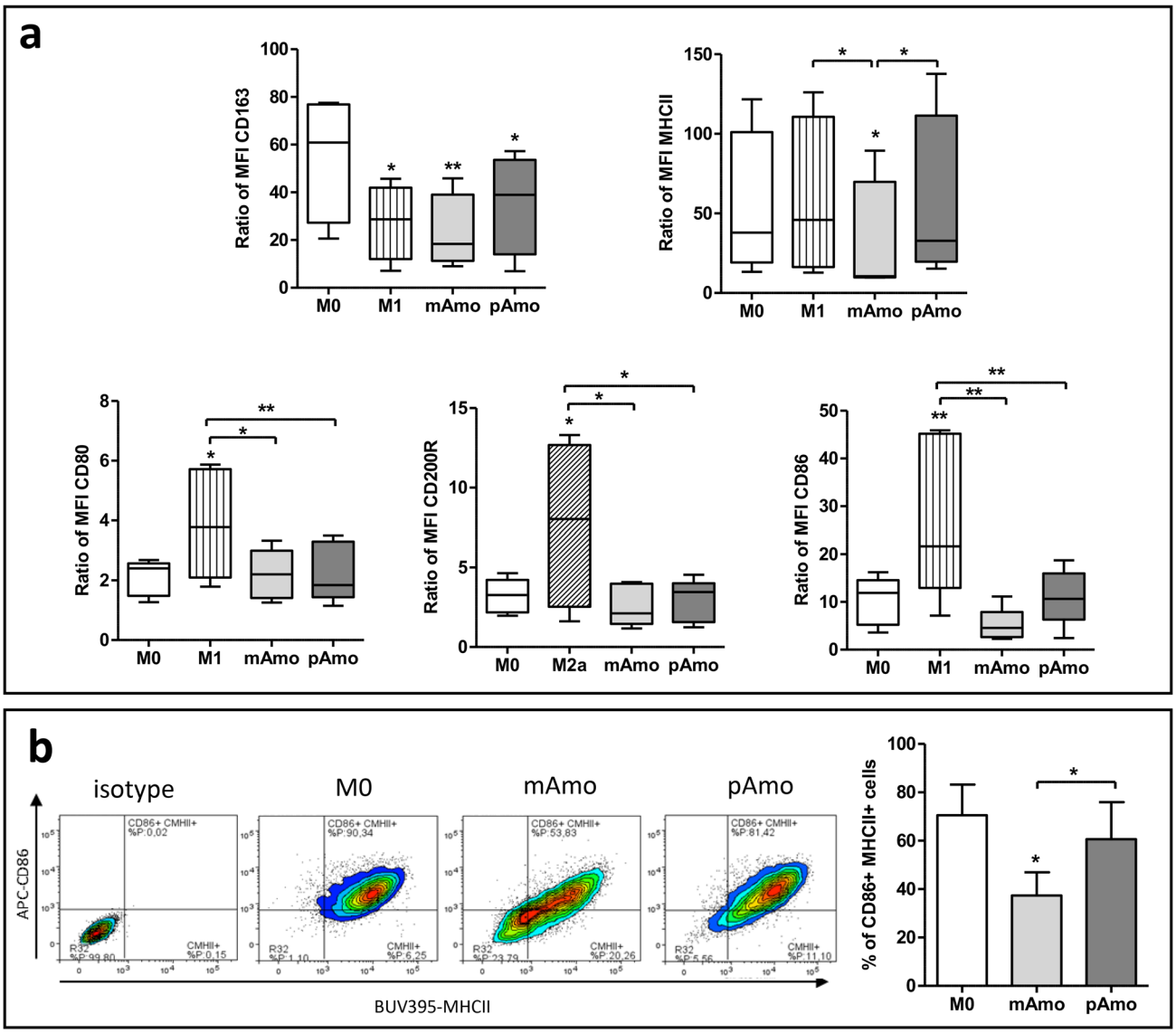

Fig. 4 Expression of polarization markers in monocyte-derived macrophages (MDMs) exposed to mAmo and pAmo. MDMs were polarized for 24 h by the addition of IFNγ/LPS (M1) or IL-4/IL-13 (M2a) or to unpolarized control cells (M0). In parallel, M0-MDMs were exposed to 20 µg/cm.^{2} of mAmo or pAmo for 24 h. Cells were harvested and stained, and the expression of cell surface molecules was analyzed by flow cytometry on viable cells. Data are expressed as MFI relative to isotype control (ratio) ± SEM for 4–5 independent experiments (**a**). Representative graph from flow cytometry showing the co-expression of CD86 and MHCII in M0 exposed or not to mAmo and pAmo (**b**). Data are expressed as the percentage of co-expressing cells ± SEM for 4 independent experiments (**b**). *$p < 0.05$, **$p < 0.01$

CD163 was associated with a decrease in the efferocytosis capacities of MDM, as previously observed in silica-exposed MDM [23], and might be due to the oversecretion of TNFα after asbestos exposure since TNFα is a cytokine known to down-regulate CD163 expression in macrophages [39]. The pro-inflammatory effects of amosite fiber exposure were confirmed by the oversecretion of two major pro-inflammatory markers, IL-8 and IL-6, in human macrophages.

In addition to inflammatory effects, pAmo also induced fibrosis. Extracellular matrix deposit is under the control of mediators such as the profibrotic molecule TGF-β1, some metalloproteinases, and their inhibitors (TIMPs). TIMP-1 overexpression considered a relevant marker of fibrosis [40] is increased after chrysotile inhalation in mice [41]. Such an increase in TIMP-1 in the BALF of pAmo-exposed mice supports the hypothesis that a non-degrading extracellular matrix environment favors fibrosis. The higher capacity of pAmo to increase lung fibrosis in comparison to mAmo confirmed previous histopathologic data collected in rodents exposed to amosite [25] or crocidolite fibers [42]. Such

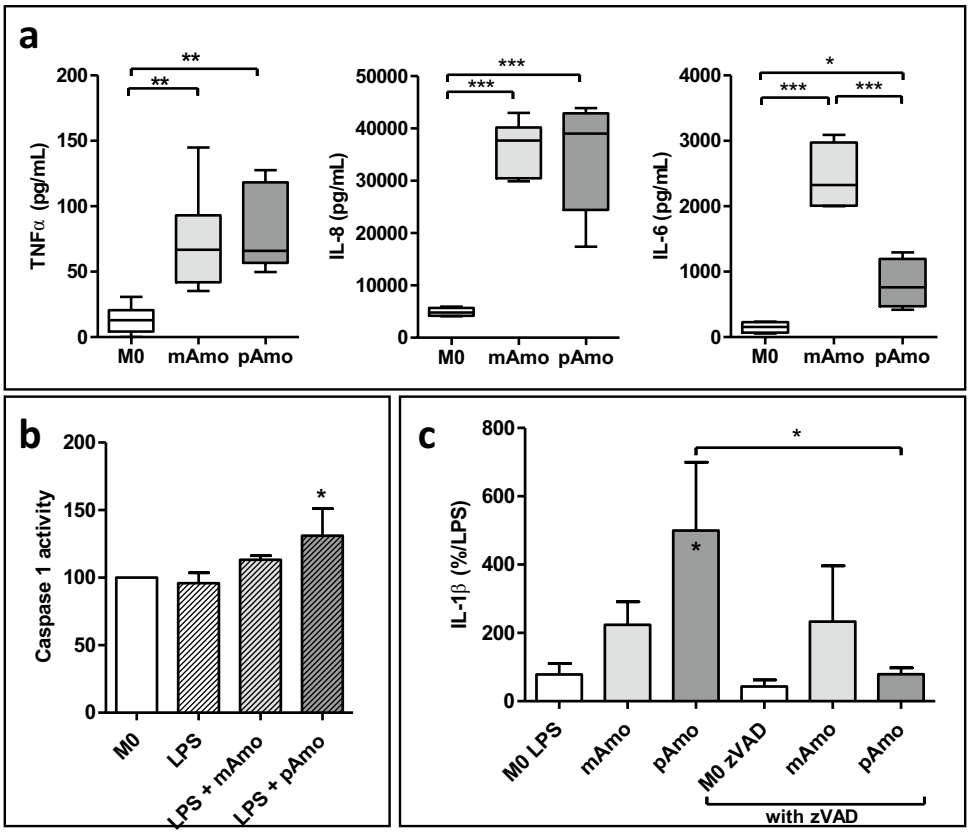

Fig. 5 Comparison of inflammatory responses of monocyte-derived macrophages (MDMs) exposed to mAmo and pAmo. MDMs were exposed to mAmo or pAmo at 20 µg/cm^2 for 24 h. Supernatants were harvested and analyzed by ELISA to determine the concentrations of some cytokines/chemokines. Data expressed in pg/ml represent the mean ± SEM of at least 4 independent experiments (**a**). MDMs were pre-treated for 4 h with LPS (10 ng/ml) in the presence of the caspase-1 inhibitor z-VAD-FMK (10 µm) (**c**) before being exposed to mAmo or pAmo at 20 µg/cm.^{2} for 2 h for the analysis of caspase-1 activity (**b**) or for 18 h for the determination of the IL-1β concentration by ELISA (**c**) as described in the "Materials and methods" section. Data expressed in percentage relative to untreated cells (M0) were the mean ± SEM of 5 independent experiments (**b**). Data expressed as a percentage of LPS-activated control cells represent the mean ± SEM of 3 independent experiments (**c**). *$p < 0.05$, **$p < 0.01$, ***$p < 0.001$

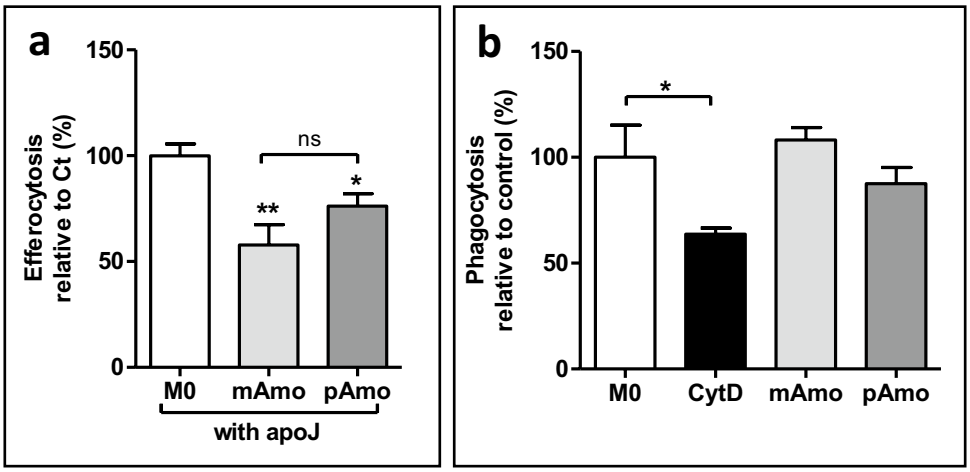

Fig. 6 Comparison of mAmo and pAmo exposure of monocyte-derived macrophages (MDMs) on efferocytosis and phagocytosis. MDMs were exposed to mAmo or pAmo at 20 µg/cm^2 for 4 h and were then exposed to apoptotic Jurkat (apoJ) cells as described in the "Materials and methods" section to evaluate their efferocytosis abilities. Data expressed in percentage relative to untreated cells (M0) were the mean ± SEM of 5 independent experiments (**a**). MDMs were exposed to mAmo or pAmo at 20 µg/cm.^{2} for 4 h or to cytochalasin D (cytD) for 1 h and then exposed to fluorescent beads for 45 min as described in the "Materials and methods" section. Data expressed in percentage relative to untreated cells (M0) were the mean ± SEM of 6 independent experiments (**b**). *$p < 0.05$, **$p < 0.01$

effects may be related to the higher pro-inflammatory properties of long fibers than short ones, notably due to frustrated macrophage phagocytosis observed with fibers longer than 10 µm [43], since chronic inflammation favors fibrosis. pAmo-induced inflammation might also favor monocyte-derived alveolar macrophage differentiation, as previously observed in asbestos-induced lung fibrosis [33].

Exposure to amphibole favors autoimmunity in humans and mice [19, 44], but, to our knowledge, no comparison of the autoimmune effects of fibers or particles according to their size and surface characteristics has been carried out to date. This could be explained by the difficulties in characterizing the size and shape of the amosite fiber workers are exposed to in epidemiological studies. The increase in seric anti-dsDNA autoantibodies found in pAmo (and not mAmo)-exposed mice is in accordance with the concomitant increase in free DNA and confirms the production of systemic autoimmune markers related to cell damage. Such data are in accordance with those showing that impaired DNase I activity increased the production of autoantibodies in systemic lupus erythematosus [45], an autoimmune disease favored by crystalline silica exposure. Crystalline silica exposure also induced self-dsDNA release in the lungs, further supporting the link between anti-dsDNA autoantibody production and free DNA release [46]. The development of an adaptive immune response is favored by the presence of danger signals such as pollutants that can promote tolerance breakdown. The adaptive immune response also depends on the nature of the antigens associated with danger signals. The presence of cell corpses related to an increase in apoptosis and/or a decrease in cell clearance also favors autoimmunity [24, 47]. Asbestos induces apoptosis [48, 49], and the decrease in efferocytosis that we observed in macrophages exposed to amosite fibers might therefore favor inflammation by both decreasing the pro-resolutive effects of efferocytic cells secreting IL-10 and by increasing the secondary necrosis followed by damage signal release. Secondary necrosis may also favor autoimmune responses after the release of auto-antigens such as DNA or nuclear proteins.

Such data are in accordance with a study showing that individuals exposed to asbestos fibers showed more DNA double-strand breaks in white blood cells and higher blood levels of anti-dsDNA antibodies than non-exposed subjects [7]. Moreover, these higher autoimmune markers observed after pAmo exposure might also be related to the greater oxidizing potential of pAmo as compared to mAmo [26, 50]. Indeed, reactive oxygen species (ROS) can generate oxidized proteins that could trigger immunogenic reactions by inducing pathogenic autoantibody release in systemic diseases such as systemic sclerosis [51]. Antigenicity is not sufficient to elicit adaptive immunity. The presentation of antigenic peptides to T cells requires the expression of co-stimulatory molecules on antigen-presenting cells. As we observed a significant decrease in MHCII and CD86 expression by mAmo-exposed human macrophages, we may hypothesize that their ability to present antigens and to activate T cells was reduced, and this may explain the lower immunoglobulin levels in BALF of mAmo-exposed mice as compared to pAmo-exposed mice, even if the dose used in vitro may not be relevant to those used in vivo. Asbestos-induced disorders of autoimmunity can also be explained by the adjuvant-type and inflammatory effects of asbestos, as also demonstrated for crystalline silica [18, 52]. The activation of macrophages by the internalization of silicate compounds favors the secretion of IL-1-β-dependent inflammasome activation and other inflammatory markers, which can then activate T-helper cells that facilitate B cell production of antibodies [53].

IgA are produced by B cells in mucosal immune systems following interaction between T cells and antigen-presenting cells that have engulfed and processed specific antigens [54]. The specific and strong increase in IgA levels in BALF of mice exposed to pAmo suggested an activation of mucosa-associated lymphoid tissue by unaltered fibers but not by milled fibers. Such an increase in IgA secretion was previously observed in the sera of a population exposed to Libby amphibole fibers [19]. An increase in IgA levels was also found in the serum and BALF of silica-inhaled lupus-prone mice [55], suggesting that these two minerals share similar mechanisms.

The results from our study and the data recently published by our group suggested that mAmo are reactive [56]. Indeed, in our in vitro analyses, mAmo reduced the percentage of double-positive CD86/MHCII MDMs and significantly decreased the efferocytosis ability of MDMs, with a stronger impact than pAmo on this parameter. Moreover, although NLRP3 activation was higher in pAmo-exposed MDMs, IL-1β secretion was also induced by mAmo. Altogether, these data suggested that mAmo are biologically reactive and have the strongest impact on some biological properties, such as efferocytosis, similar to what was observed in silica-exposed MDMs [23], further linking silica and amosite. These effects on efferocytosis may be related to the fact that mAmo, similarly to silica, are particles, and this result suggested that beyond the size of the fibers, the presence of particles is also important to explain the biological effects. These data are in accordance with Davis et al. [25], Tomatis et al. [26], Graham et al. and Gilmour et al. [27, 57], and more recently, Leinardi et al. [56], demonstrating that the biological and toxicological effects of mAmo should not be neglected. Their impact in vivo on other biological processes such as asbestos-related cancers should be further explored. The biopersistence and trafficking of mAmo fibers and particles in vivo also deserve further experiments.

The asbestos concentration used in vivo (100 µg), time of analysis post-exposure (4 months), and sex of mice (female)

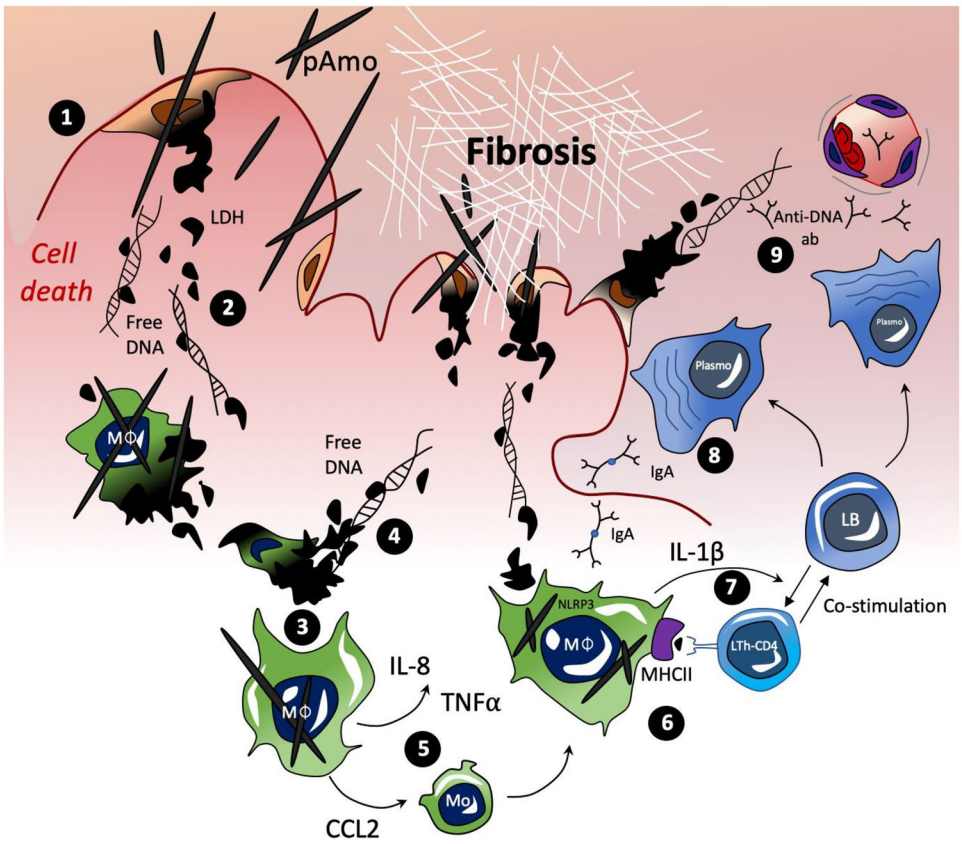

Fig. 7 Autoimmune effects of pAmo could be triggered by (1) pAmo-induced cell death associated with (2) a release of autoantigens and free DNA, favored by (3) a defect of efferocytosis leading to the (4) accumulation of residual cell corpses with secondary necrosis. pAmo also induced (5) the release of IL-8 and TNFα by macrophages (Mϕ) and CCL-2 in the alveolar lumen, with potential recruitment of monocytes (Mo), increasing lung inflammation. Autoantigens can be (6) presented to lymphocyte Th-CD4 through MHCII since its expression is preserved after pAmo exposure by contrast to mAmo exposure. Immune activation after pAmo exposure is also favored by (7) adjuvant effect (NLRP3 inflammasome) of pAmo, leading to a release of IL-1β. Such pathogenic events could elicit an elevation of (8) local IgA in the lungs and (9) systemic autoantibody production, favored by the chronic persistence of pAmo in the lung

were selected on the basis of previous studies evaluating asbestos-induced autoimmunity [12, 44, 58, 59]. We may think that such autoimmunity could be triggered at lower concentrations of asbestos fibers, as shown by Zebedeo et al. [12] after an exposure of 60 µg of amphibole. As immune response may differ depending on sex and as autoimmunity is more frequent in females than in males [60], we cannot exclude the different results on autoimmunity that could be observed in males.

To conclude, our results confirmed the higher lung pathogenicity of pAmo as compared to mAmo in the mouse model. Altogether, we hypothesize that autoimmune effects of pAmo may be sequenced (a) by cell death associated with a defect of efferocytosis that favors an accumulation of residual cell corpses and a subsequent secondary necrosis, which represents a source of autoantigens, and (b) by immune activation via the adjuvant effect (NLRP3 inflammasome) of long fibers, leading to antigen presentation. Such pathogenic events could elicit an elevation of local IgA and systemic autoantibody production (i.e., anti-dsDNA autoantibodies), favored by the chronic persistence of pAmo in the lungs (Fig. 7). Our results suggest that the size reduction of amosite fibers leading to surface characteristic modifications due to grinding reduces the risk of developing systemic autoimmunity in vivo. A careful assessment of autoimmune features in patients exposed to pAmo or to elongated mineral particles of interest (length less than 5 µm) might be proposed for early detection of autoimmune diseases and early treatment before irreversible damages appear. However, the impact and toxicity of mAmo should not be neglected, as the amosite particles contained in mAmo, obtained after grinding, also have an impact on important biological processes such as efferocytosis and co-stimulation markers. Beyond autoimmunity, these effects could play a role in other amosite-related hazards, such as asbestos-induced cancers, warranting further in vivo and mechanistic experiments in the future.

Supplementary Information The online version contains supplementary material available at https://doi.org/10.1007/s00109-023-02401-9.

Acknowledgements The authors thank the platform of flow cytometry (Biosit, Rennes, France) and the nurses, medical team, and patients from the "Service de Santé au Travail et Pathologie Professionnelle" and V. Visseiche and K. Coat of Rennes University Hospital (France).

Author contribution The authors that contributed to the study conception and design were AL, FH, and VL. Material preparation, data collection, and analysis were performed by AL, RL, KP, YY, FT, CP, AP, NB, ML, ELT, ED, FH, and VL. The first draft of the manuscript was written by VL and AL, and all authors commented on previous versions of the manuscript. All authors read and approved the final manuscript.

Funding This work was supported by the "Agence Nationale de sécurité sanitaire de l'alimentation, de l'environnement et du travail" (Anses) (MacFibOsis project no. 2018/1/149), the Institut National de la Santé et de la Recherche Médicale (INSERM), the Université de

Rennes (Univ Rennes), "Actions de Recherche Concertées, Fédération Wallonie-Bruxelles" (ARC 19/24-098, CYTAID), "Fondation Contre le Cancer" (2019-219), and the European Commission under the H2020 project (Contract no. 874707, Eximious). FT kindly acknowledges the financial support from the BRIC 2019 project "Caractterizzazione cristallochimica e studio della reattività de superficie di fibre menerali di interesse ambiantale e sanitario ai fini di un'accurata analisa del rischio di contaminazione" funded by INAIL with grant number ID 57.1. FH is a Senior Research Associate with the FNRS, Belgium.

Availability of data and material The datasets generated during and/or analyzed during the current study are available from the corresponding author on reasonable request.

Declarations

Ethics approval and consent to participate The use of human samples and animal studies was approved by the Committee for Protection of Persons (approval Ile de France 5, no. 2020-A01990-39) and the Institutional Animal Care and Use Committee (EEC nos. 86/609, LA1230312, and 2018/UCL/MD/012), respectively.

Competing interests The authors declare no competing interests.

References

1. Stayner L, Welch LS, Lemen R (2013) The worldwide pandemic of asbestos-related diseases. Annu Rev Public Health 34:205–216. https://doi.org/10.1146/annurev-publhealth-031811-124704
2. IARC (2012) IARC, Monographs on the Evaluation of Carcinogenic Risks to Humans. Arsenic, Metals, Fibres, and Dusts. A Review of Human Carcinogens, 2012
3. Thives LP, Ghisi E, Thives Júnior JJ, Vieira AS (2022) Is asbestos still a problem in the world? A current review J Environ Manage 319:115716. https://doi.org/10.1016/j.jenvman.2022.115716
4. USGS (2012) Asbestos Statistics and Information | U.S. Geological Survey. https://www.usgs.gov/centers/national-minerals-information-center/asbestos-statistics-and-information
5. Cullinan P, Muñoz X, Suojalehto H et al (2017) Occupational lung diseases: from old and novel exposures to effective preventive strategies. Lancet Respir Med 5:445–455. https://doi.org/10.1016/S2213-2600(16)30424-6
6. EMPs, NIOSH (2011) Current intelligence bulletin 62: asbestos fibers and other elongate mineral particles: state of the science and roadmap for research. https://doi.org/10.26616/NIOSHPUB2011159
7. Marczynski B, Czuppon AB, Marek W et al (1994) Increased incidence of DNA double-strand breaks and anti-ds DNA antibodies in blood of workers occupationally exposed to asbestos. Hum Exp Toxicol 13:3–9. https://doi.org/10.1177/096032719401300102
8. Pfau JC, Serve KM, Noonan CW (2014) Autoimmunity and asbestos exposure Autoimmune Dis 2014:782045. https://doi.org/10.1155/2014/782045
9. Janssen LMF, Ghosh M, Lemaire F et al (2022) Exposure to silicates and systemic autoimmune-related outcomes in rodents: a systematic review. Part Fibre Toxicol 19:4. https://doi.org/10.1186/s12989-021-00439-6
10. Webber MP, Moir W, Zeig-Owens R et al (2015) Nested case-control study of selected systemic autoimmune diseases in World Trade Center rescue/recovery workers. Arthritis Rheumatol 67:1369–1376. https://doi.org/10.1002/art.39059
11. Cavalin C, Lescoat A, Sigaux J et al (2022) Crystalline silica exposure in patients with rheumatoid arthritis and systemic sclerosis: a nationwide cross-sectional survey. Rheumatology (Oxford) keac675. https://doi.org/10.1093/rheumatology/keac675
12. Zebedeo CN, Davis C, Peña C et al (2014) Erionite induces production of autoantibodies and IL-17 in C57BL/6 mice. Toxicol Appl Pharmacol 275:257–264. https://doi.org/10.1016/j.taap.2014.01.018
13. Fubini B (1997) Surface reactivity in the pathogenic response to particulates. Environ Health Perspect 105(Suppl 5):1013–1020. https://doi.org/10.1289/ehp.97105s51013
14. Donaldson K, Seaton A (2012) A short history of the toxicology of inhaled particles. Part Fibre Toxicol 9:13. https://doi.org/10.1186/1743-8977-9-13
15. Boulanger G, Andujar P, Pairon J-C et al (2014) Quantification of short and long asbestos fibers to assess asbestos exposure: a review of fiber size toxicity. Environ Health 13:59. https://doi.org/10.1186/1476-069X-13-59
16. Dodson RF, Atkinson MAL, Levin JL (2003) Asbestos fiber length as related to potential pathogenicity: a critical review. Am J Ind Med 44:291–297. https://doi.org/10.1002/ajim.10263
17. Murthy S, Larson-Casey JL, Ryan AJ et al (2015) Alternative activation of macrophages and pulmonary fibrosis are modulated by scavenger receptor, macrophage receptor with collagenous structure. FASEB J 29:3527–3536. https://doi.org/10.1096/fj.15-271304
18. Dostert C, Pétrilli V, Van Bruggen R et al (2008) Innate immune activation through Nalp3 inflammasome sensing of asbestos and silica. Science 320:674–677. https://doi.org/10.1126/science.1156995
19. Pfau JC, Sentissi JJ, Weller G, Putnam EA (2005) Assessment of autoimmune responses associated with asbestos exposure in Libby, Montana, USA. Environ Health Perspect 113:25–30. https://doi.org/10.1289/ehp.7431
20. Bunderson-Schelvan M, Pfau JC, Crouch R, Holian A (2011) Nonpulmonary outcomes of asbestos exposure. J Toxicol Environ Health B Crit Rev 14:122–152. https://doi.org/10.1080/10937404.2011.556048
21. Parks CG, Conrad K, Cooper GS (1999) Occupational exposure to crystalline silica and autoimmune disease. Environ Health Perspect 107(Suppl 5):793–802. https://doi.org/10.1289/ehp.99107s5793
22. Pollard KM (2016) Silica, silicosis, and autoimmunity. Front Immunol 7. https://doi.org/10.3389/fimmu.2016.00097
23. Lescoat A, Ballerie A, Lelong M et al (2020) Crystalline silica impairs efferocytosis abilities of human and mouse macrophages: implication for silica-associated systemic sclerosis. Front Immunol 11:219. https://doi.org/10.3389/fimmu.2020.00219
24. Kawano M, Nagata S (2018) Efferocytosis and autoimmune disease. Int Immunol 30:551–558. https://doi.org/10.1093/intimm/dxy055
25. Davis JM, Addison J, Bolton RE et al (1986) The pathogenicity of long versus short fibre samples of amosite asbestos administered to rats by inhalation and intraperitoneal injection. Br J Exp Pathol 67:415–430
26. Tomatis M, Turci F, Ceschino R et al (2010) High aspect ratio materials: role of surface chemistry vs. length in the historical "long and short amosite asbestos fibers." Inhal Toxicol 22:984–998. https://doi.org/10.3109/08958378.2010.504243
27. Graham A, Higinbotham J, Allan D et al (1999) Chemical differences between long and short amosite asbestos: differences in oxidation state and coordination sites of iron, detected by infrared spectroscopy. Occup Environ Med 56:606–611. https://doi.org/10.1136/oem.56.9.606
28. Arras M, Huaux F, Vink A et al (2001) Interleukin-9 reduces lung fibrosis and type 2 immune polarization induced by silica particles in a murine model. Am J Respir Cell Mol Biol 24:368–375. https://doi.org/10.1165/ajrcmb.24.4.4249

29. Biondi PA, Chiesa LM, Storelli MR, Renon P (1997) A new procedure for the specific high-performance liquid chromatographic determination of hydroxyproline. J Chromatogr Sci 35:509–512. https://doi.org/10.1093/chromsci/35.11.509
30. Lescoat A, Lelong M, Jeljeli M et al (2020) Combined anti-fibrotic and anti-inflammatory properties of JAK-inhibitors on macrophages in vitro and in vivo: perspectives for scleroderma-associated interstitial lung disease. Biochem Pharmacol 178:114103. https://doi.org/10.1016/j.bcp.2020.114103
31. Ballerie A, Lescoat A, Augagneur Y et al (2019) Efferocytosis capacities of blood monocyte-derived macrophages in systemic sclerosis. Immunol Cell Biol 97:340–347. https://doi.org/10.1111/imcb.12217
32. Liu G, Beri R, Mueller A, Kamp DW (2010) Molecular mechanisms of asbestos-induced lung epithelial cell apoptosis. Chem Biol Interact 188:309–318. https://doi.org/10.1016/j.cbi.2010.03.047
33. Joshi N, Watanabe S, Verma R et al (2020) A spatially restricted fibrotic niche in pulmonary fibrosis is sustained by M-CSF/M-CSFR signalling in monocyte-derived alveolar macrophages. Eur Respir J 55:1900646. https://doi.org/10.1183/13993003.00646-2019
34. Jaguin M, Fardel O, Lecureur V (2015) Exposure to diesel exhaust particle extracts (DEPe) impairs some polarization markers and functions of human macrophages through activation of AhR and Nrf2. PLoS One 10:e0116560. https://doi.org/10.1371/journal.pone.0116560
35. Speil S, Leineweber JP (1969) Asbestos minerals in modern technology. Environ Res 2:166–208. https://doi.org/10.1016/0013-9351(69)90036-x
36. Bernstein DM (2022) The health effects of short fiber chrysotile and amphibole asbestos. Crit Rev Toxicol 52:89–112. https://doi.org/10.1080/10408444.2022.2056430
37. Li M, Gunter ME, Fukagawa NK (2012) Differential activation of the inflammasome in THP-1 cells exposed to chrysotile asbestos and Libby "six-mix" amphiboles and subsequent activation of BEAS-2B cells. Cytokine 60:718–730. https://doi.org/10.1016/j.cyto.2012.08.025
38. Palomäki J, Välimäki E, Sund J et al (2011) Long, needle-like carbon nanotubes and asbestos activate the NLRP3 inflammasome through a similar mechanism. ACS Nano 5:6861–6870. https://doi.org/10.1021/nn200595c
39. Buechler C, Ritter M, Orsó E et al (2000) Regulation of scavenger receptor CD163 expression in human monocytes and macrophages by pro- and antiinflammatory stimuli. J Leukoc Biol 67:97–103
40. Manoury B, Caulet-Maugendre S, Guénon I et al (2006) TIMP-1 is a key factor of fibrogenic response to bleomycin in mouse lung. Int J Immunopathol Pharmacol 19:471–487. https://doi.org/10.1177/039463200601900303
41. Sabo-Attwood T, Ramos-Nino ME, Eugenia-Ariza M et al (2011) Osteopontin modulates inflammation, mucin production, and gene expression signatures after inhalation of asbestos in a murine model of fibrosis. Am J Pathol 178:1975–1985. https://doi.org/10.1016/j.ajpath.2011.01.048
42. Adamson IY, Bowden DH (1987) Response of mouse lung to crocidolite asbestos. 1. Minimal fibrotic reaction to short fibres. J Pathol 152:99–107. https://doi.org/10.1002/path.1711520206
43. Schinwald A, Donaldson K (2012) Use of back-scatter electron signals to visualise cell/nanowires interactions in vitro and in vivo; frustrated phagocytosis of long fibres in macrophages and compartmentalisation in mesothelial cells in vivo. Part Fibre Toxicol 9:34. https://doi.org/10.1186/1743-8977-9-34
44. Pfau JC, Sentissi JJ, Li S et al (2008) Asbestos-induced autoimmunity in C57BL/6 mice. J Immunotoxicol 5:129–137. https://doi.org/10.1080/15476910802085756
45. Gajic-Veljic M, Bonaci-Nikolic B, Lekic B et al (2015) Importance of low serum DNase I activity and polyspecific anti-neutrophil cytoplasmic antibodies in propylthiouracil-induced lupus-like syndrome. Rheumatology (Oxford) 54:2061–2070. https://doi.org/10.1093/rheumatology/kev243
46. Benmerzoug S, Rose S, Bounab B et al (2018) STING-dependent sensing of self-DNA drives silica-induced lung inflammation. Nat Commun 9:5226. https://doi.org/10.1038/s41467-018-07425-1
47. Abdolmaleki F, Farahani N, Gheibi Hayat SM et al (2018) The role of efferocytosis in autoimmune diseases. Front Immunol 9:1645. https://doi.org/10.3389/fimmu.2018.01645
48. Hamilton RF, Iyer LL, Holian A (1996) Asbestos induces apoptosis in human alveolar macrophages. Am J Physiol 271:L813-819. https://doi.org/10.1152/ajplung.1996.271.5.L813
49. Liu W, Ernst JD, Broaddus VC (2000) Phagocytosis of crocidolite asbestos induces oxidative stress, DNA damage, and apoptosis in mesothelial cells. Am J Respir Cell Mol Biol 23:371–378. https://doi.org/10.1165/ajrcmb.23.3.4094
50. Riganti C, Aldieri E, Bergandi L et al (2003) Long and short fiber amosite asbestos alters at a different extent the redox metabolism in human lung epithelial cells. Toxicol Appl Pharmacol 193:106–115. https://doi.org/10.1016/s0041-008x(03)00339-9
51. Servettaz A, Goulvestre C, Kavian N et al (2009) Selective oxidation of DNA topoisomerase 1 induces systemic sclerosis in the mouse. J Immunol 182:5855–5864. https://doi.org/10.4049/jimmunol.0803705
52. Otsuki T, Maeda M, Murakami S et al (2007) Immunological effects of silica and asbestos. Cell Mol Immunol 4:261–268
53. Eisenbarth SC, Colegio OR, O'Connor W et al (2008) Crucial role for the Nalp3 inflammasome in the immunostimulatory properties of aluminium adjuvants. Nature 453:1122–1126. https://doi.org/10.1038/nature06939
54. Corthésy B (2013) Multi-faceted functions of secretory IgA at mucosal surfaces. Front Immunol 4:185. https://doi.org/10.3389/fimmu.2013.00185
55. Rajasinghe LD, Li Q-Z, Zhu C et al (2020) Omega-3 fatty acid intake suppresses induction of diverse autoantibody repertoire by crystalline silica in lupus-prone mice. Autoimmunity 53:415–433. https://doi.org/10.1080/08916934.2020.1801651
56. Leinardi R, Rita Petriglieri J, Pochet A et al (2023) Distinct pro-inflammatory mechanisms elicited by short and long amosite asbestos fibers in macrophages. Int J Mol Sci 15145–15161. https://doi.org/10.3390/ijms242015145
57. Gilmour PS, Brown DM, Beswick PH et al (1997) Free radical activity of industrial fibers: role of iron in oxidative stress and activation of transcription factors. Environ Health Perspect 105(Suppl 5):1313–1317. https://doi.org/10.1289/ehp.97105s51313
58. Pfau JC, Li S, Holland S, Sentissi JJ (2011) Alteration of fibroblast phenotype by asbestos-induced autoantibodies. J Immunotoxicol 8:159–169. https://doi.org/10.3109/1547691X.2011.562257
59. Ferro A, Zebedeo CN, Davis C et al (2014) Amphibole, but not chrysotile, asbestos induces anti-nuclear autoantibodies and IL-17 in C57BL/6 mice. J Immunotoxicol 11:283–290. https://doi.org/10.3109/1547691X.2013.847510
60. Klein SL, Flanagan KL (2016) Sex differences in immune responses. Nat Rev Immunol 16:626–638. https://doi.org/10.1038/nri.2016.90

Authors and Affiliations

Alain Lescoat[1,2] · Riccardo Leinardi[3] · Kévin Pouxvielh[1] · Yousof Yakoub[3] · Marie Lelong[1] · Amandine Pochet[3] · Erwan Dumontet[4] · Nessrine Bellamri[1] · Erwan Le Tallec[1,2] · Cristina Pavan[5,6] · Francesco Turci[5,6] · Christophe Paris[1,7] · François Huaux[3] · Valérie Lecureur[1,8]

✉ Valérie Lecureur
valerie.lecureur@univ-rennes.fr

1 Univ Rennes, CHU Rennes, INSERM, EHESP, IRSET (Institut de Recherche en Santé, environnement et travail)—UMR_S 1085, 35000 Rennes, France

2 Department of Internal Medicine & Clinical Immunology, Rennes University Hospital, 35000 Rennes, France

3 Louvain Centre for Toxicology and Applied Pharmacology (LTAP), Institut de Recherche Expérimentale Et Clinique (IREC), Université Catholique de Louvain (UCL), Avenue Hippocrate 57, Bte B-1.57.06, 1200 Brussels, Belgium

4 CHU Rennes, Pôle de Biologie, Rennes, France

5 "G. Scansetti" Interdepartmental Center for Studies On Asbestos and Other Toxic Particulates, University of Turin, Via Pietro Giuria 7, 10125 Turin, Italy

6 Department of Chemistry, University of Turin, Via Pietro Giuria 7, 10125 Turin, Italy

7 Service de Santé Au Travail Et Pathologie Professionnelle, CHU Rennes, 35000 Rennes, France

8 UMR-INSERM 1085, Campus Santé, 2 Avenue du Pr Léon Bernard, 35043 Rennes Cedex, France